Optimum sintering method and temperature for cold compact Bismuth Telluride pellets for thermoelectric applications

Farheen F. Jaldurgam [a,b], Zubair Ahmad [b,c,*], Farid Touati [a], Abdulla Al Ashraf [c], Abdul Shakoor [c], Jolly Bhadra [b], Noora J. Al-Thani [b], Dong Suk Han [c], Talal Altahtamouni [d]

[a] Department of Electrical Engineering, College of Engineering, Qatar University, 2713 Doha, Qatar
[b] Qatar University Young Scientist Center (QUYSC), Qatar University, 2713 Doha, Qatar
[c] Center for Advanced Materials (CAM), Qatar University, 2713 Doha, Qatar
[d] Materials Science & Technology Program, College of Arts and Sciences, Qatar University, 2713 Doha, Qatar

ARTICLE INFO

ABSTRACT

This work intends to investigate the optimum sintering method and temperature that can improve the efficiency of bismuth telluride cold compact pellets, for the thermoelectric applications. Different p-type and n-type bismuth telluride cold compact pellets were treated using three different sintering techniques and conditions: pressure less (conventional), microwave, and tube (using argon environment) at temperatures 250 °C, 300 °C, 350 °C, and 400 °C. The structural, microscopic, electron transport, thermal, and dielectric properties of the pristine and sintered samples were examined. Broadband dielectric spectroscopy was performed to extract a detailed picture of the dielectric properties of the samples. Even though each type of sintering had its own merits and demerits, the optimum conditions for enhanced electric and thermal features were found in microwave furnace followed by tube and conventional. Low thermal conductivity of 0.4 W/m/K was observed in the samples sintered at 250 °C while the increase in sintering temperature from 250 °C to 300 °C improved the crystallinity of the material. Moreover, the crystal structure of the bismuth telluride altered with the occurrence of higher oxidation leading to the formation of high bismuth telluride oxide phases at sintering temperatures above 300 °C, more dominantly in the n-type samples.

1. Introduction

Thermoelectrics have paved the way to utilize the underutilized and often considered heat waste by converting it into electricity. Nanostructured thermoelectric materials have comparatively improved thermoelectric performance and find themselves in enormous potential applications from the TEG to cooling and various other purposes [1]. The Phonon-Glass-Electron-crystal effect dictates that for a material to be an ideal thermoelectric, it must possess the electronic conduction properties of a crystal and thermal conduction properties of a glass [2]. Better thermoelectric performance is achieved in the material with high electric conduction and low thermal conduction [3–7].

Bismuth telluride (Bi_2Te_3) is the first and best thermoelectric material to be developed for refrigeration and cooling purposes due to its immense capability of converting waste heat to beneficial electrical energy [8]. Many works have aimed to increase the performance of the nanostructured bismuth telluride by increasing the electrical conductivity, Seebeck coefficient, and power factor or by decreasing the thermal conductivities [9–13]. Bi_2Te_3 is basically a compound element of Bi (Bismuth) and Te (Tellurium) [14]. The behavior of bismuth physically is of metal but alloyed with tellurium, and it functions as a semiconductor TE material [15]. Bi_2Te_3 operates in the low to intermediate temperature range [16]. A factor determines the efficiency of thermoelectric material called the "Figure of Merit (ZT)," which is given by [17],

$$ZT = \left(\frac{\alpha^2 \sigma}{\kappa} \right) T \tag{1}$$

where, σ, κ, and α are electrical conductivity, thermal conductivity, and Seebeck coefficient, respectively.

The overall efficiency of a thermoelectric cell relies on the ZT value of the p-type and n-type TE material. Immense efforts have been made to improve the ZT, such as nanostructuring [16], forming thin films [18], doping [19], alloying [20], increasing the grain boundaries [21], optimizing the synthesis conditions [22], and so on. It has also been a goal to replicate and reproduce such high-performance thermoelectrics on a large scale at affordable rates and conditions [23]. The enhancement has been achieved up to some level by successfully increasing the phonon scattering at the grain boundaries and quantum confinement [24]. Bismuth telluride functions efficiently at low temperatures and is also available commercially for practical applications. Due to the delicate and high volatile nature of tellurium at high temperatures, the conventional processes do not yield the desired results [25]. It is necessary to inquire about the optimum conditions for bismuth telluride that has the benefits of performance, cost, reliability, and time.

Sintering has the proven practical advantage of producing better polycrystalline forms of the material [26]. Sintering reduces the lattice conductivity of the material, and bulk nanostructures can be easily realized [27]. But there is a reduction in the power factor in the sintered materials, and the benefit of lattice conductivity reduction is overshadowed unless some measure of crystal alignment or orientation is achieved [28]. Conventional or pressureless sintering is the simplest sintering form that involves heating of the ambient temperature prepared powder compact without any applied external pressure [29]. On the other hand, in microwave sintering or non-conventional sintering, the nature of the heat transfer mechanism is considerably different and occurs in terms of convection, radiation, and conduction [30].

Zhou et al. [31] used the microwave-assisted polyol method to synthesize nanocrystalline Bi_2Te_3 with a combination of nanorods and hexagonal nanoflakes of length ranging from 200 to 400 nm and 90–150 nm, respectively. Kim et al. [32] used three different methods, namely the chemical reaction method, conventional pulverization method, and gas atomization method, to prepare the starting powders of nanostructured Bi_2Te_3 alloys. In the traditional pulverization method, the materials bismuth, tellurium, and antimony were mixed and treated in a quartz tube at 1000 °C temperature for 24 h. Their work suggested better crystal orientation alignment for enhanced TE characteristics. High-quality bismuth selenide (Bi_2Se_3) single-crystalline bulk TE materials were synthesized in a 12-inch horizontal quartz tube furnace and heated in the 450–580 °C temperature range for 1–5 h [33]. Ashalley et al. reviewed in detail the characteristics and synthesis methods to realize various nanostructured Bi_2Te_3 materials (0D, 1D, 2D, and nanocomposites) [34]. Anandan et al. [35] investigated the influence of sintering temperature on the phase transformation and morphological evolution in a wet chemical synthesized Bi_2Te_3 nanocrystal pellets. Phase change to BiTe was observed at high sintering temperatures, and this BiTe phase dominated the Bi_2Te_3 phase at 773 K. Usually, the chemical methods lack efficient reproducibility in bulk production [36].

Comparisons of the impact of different sintering and sintering temperature on the morphological, phase, thermal and dielectric properties of the cold compact pellets have not been investigated before, and our work aims to fill that gap. This work is primarily divided into three parts. In the first part, we have treated both p-type and n-type samples using three different types of sintering, namely, conventional, microwave, and tube. In the second part, we have done several characterizations: structural, electrical, thermal, and microscopic, of the prepared samples. Finally, we have done broadband dielectric spectroscopy analysis to exhaustively study the dielectric properties of the samples.

2. Experimental details

2.1. Sample preparation

The materials used to prepare samples are the commercially available p-type and n-type bismuth telluride powders (Bi_2Te_3 -purity:99.99% and size: 200 mesh) supplied by Nanoshel LLC (NS6130-12-000436A). The p-type powders were bismuth telluride doped with antimony, and n-type powders were bismuth telluride with indium sulfide doping. The powders were weighed to be 5 g each, and then various p-type and n-type pellets were compacted by cold uniaxial pressing under an applied pressure of 6 MPa for 30 s. Each pellet prepared was of diameter and width 13 mm and 3 mm, respectively and the density of the pellets was 12.56 ± 0.04 g/mm³. These samples were then sintered in conventional or box furnace, tube furnace, and microwave furnace at temperatures 250 °C, 300 °C, 350 °C, and 400 °C. In the tube furnace, the sintering is done in the presence of argon gas flow. In all the cases, the heating ramp time is considered as 10 °C/min. At each temperature, the samples were sintered for 1 h and left to be cooled down to room temperature and then removed from their respective chambers. The sintered samples
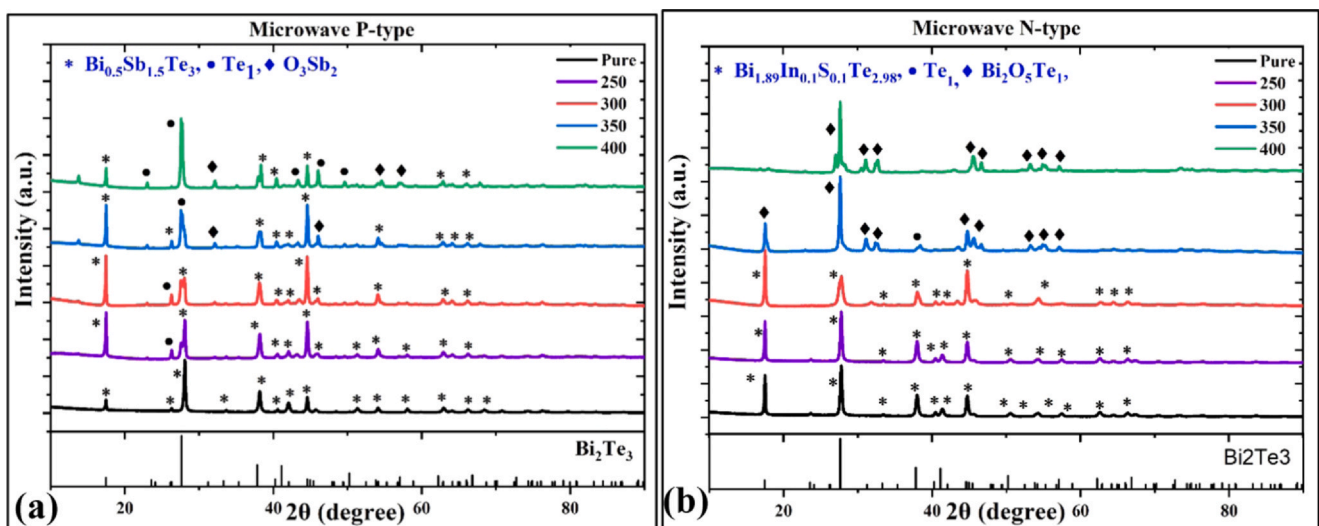

Fig. 1. XRD profile of (a) microwave sintered p-type Bi_2Te_3, and (b) microwave n-type Bi_2Te_3.

were then investigated for structural, microscopic, electric, and thermal properties.

2.2. Characterization

The various samples from the sintered and non-sintered pure pellets were subjected to XRD analysis (X-ray powder diffraction). The XRD patterns were logged over the range of 2θ between 10° and 90°, using PANAnalytical EMPYREAN, Netherland (45 kV/40 mA) with radiation of CuKα1 (λ = 1.540598 Å) and CuKα2 (λ = 1.544426 Å). A Nova Nano Scanning Electron Microscopy (Model: Nova Nano SEM 450, Manufacturer: FEI, Netherland) was used for Field emission scanning electron microscopy (FESEM) to analyze the morphological and chemical composition changes of bismuth and tellurium in the sintered materials along with detection of oxide concentrations. The Ossila four-point probe system recorded the DC electrical conductivities. The Broadband Dielectric Spectroscopy analysis determined the electrical characteristics such as impedance, AC electrical conductivities, dielectric permittivity, electric modulus, specific resistance, and phase angle. This was done using Novocontrol GmbH Concept 40 broadband dielectric spectrometer. The different parameters were computed using Novocontrol Win DETA software. The data from the samples were collected over the frequency range of 10–10 MHz at fixed temperatures in the range of 25 °C to 375 °C with a 25 °C temperature increment. The thermal characteristics such as thermal conductivity, specific heat capacity, and thermal diffusivity were determined by thermal constants analyzer (TCA) test using the TPS 2500 s hot disk analyzer.

3. Results and discussion

3.1. Structural characterization

Fig. 1 shows the XRD profile of all the samples treated through the microwave sintering method at different temperatures. To study, analyze and compare the structural behavior, bonding, and impurity phase changes of Bi_2Te_3 at different sintering temperatures, powder X-ray diffraction data were collected from 26 Bi_2Te_3 samples using Cu-Kα radiation. Out of the 26 samples, two were pristine p-type and n-type samples, and others were sintered samples at temperatures 250 °C, 300 °C, 350 °C, and 400 °C in the box, microwave, and tube furnace, respectively. The XRD analysis data were collected in the 2θ range from 10° to 90°. Bragg's peaks and fitted profile for all the samples are shown in Fig. 1. The grain size calculations of the different sample XRD profiles are given in the Supplementary Data file. The grain size was approximated through the Debye-Scherrer formula [37],

$$D = \frac{k\lambda}{\beta.\cos\theta} \tag{2}$$

where D is the crystallite size in nm, k is the shape factor (0.93), λ is the wavelength of X-ray and in this case, CuKα (1.54 nm), β is the FWHM (full width half maximum) of the intense peak in radians, and θ is the Braggs angle.

The pure p-type samples consisted of a pure single phase of antimony bismuth telluride ($Bi_{0.5}Sb_{1.5}Te_3$) with hexagonal structure as confirmed by ICDD: 98–061–7062 data whereas the n-type samples comprised of a pure single phase of bismuth indium sulfide telluride ($Bi_{1.894}In_{0.106}S_{0.11}Te_{2.89}$) with hexagonal structure as confirmed by ICDD: 98–065–8770 data. The p-type material was made by doping bismuth telluride with antimony and n-type samples were made by doping bismuth telluride with indium sulfide.

For the p-type samples in conventional sintering, the pristine and BP250 showed sharp peaks indicating high crystalline nature. Peak broadening can be observed at 2θ = 27.6 with (0 1 5) plane in BP300 and BP350 samples, and this may be due to descent in size of the

crystallite with the increase in sintering temperature up to 350 °C. But in the sample BP400, as shown in Fig. S1(b) (Supplementary Data), peak shifts can be observed due to the introduction of the oxidized impure phase of $Bi_1O_4Sb_1$ as confirmed by ICDD:98-007-5901. There have also been changes in peak position and intensities above 350 °C temperatures. On the contrary, in the case of n-type Bi_2Te_3, the peaks and phases are similar for pristine, BN250, and BN300 samples. But whereas for the samples BN350 and BN400, there are various new peaks at different 2θ indicated by several impure phases such as $Bi_2O_5Te_1$, $Bi_2O_7Te_2$, and $Bi_2O_{11}Te_4$ as seen in Fig. S1(c) (Supplementary Data) that can be confirmed by ICDD:98-028-0627, 98-008-5725 and 98-007-2709. It is also noteworthy that as the sintering temperature increased, there has been an exponential increase in the various oxide phases. To summarize, it can be said that the p-type samples are pure single-phase and crystalline until sintering temperature 350 °C and have oxide impure phase at temperatures beyond it. On the other hand, in the n-type samples, the impure phases have been introduced at a lower sintering temperature of 350 °C. The estimated grain size (from the Supplementary Data) indicates that the crystallite size decreased as the sintering temperature increased. It can be vividly deduced that the size of the sub-microns depends on the sintering temperature. The size of the sub-microns range from 400 nm to 1000 nm.

In the microwave furnace, the p-type samples have an almost similar XRD profile for all the samples, as shown in Fig. 1(a). There has been a slight increase in intensities and some broadening at some peaks with some negligible shift in the phases. Also, oxidations phases are from low to null in the p-type samples. On the contrary, in the n-type material, the profile is similar for pristine, MN250, and MN300 samples with pure single phases whereas, there are some considerable amounts of impure bismuth oxide phase of $Bi_2O_5Te_1$ in MN400 as depicted in Fig. 1(b) and confirmed by ICDD:98-028-0627. Overall, the p-type material in the microwave furnace has been stable and did not change any phase through temperatures 250 °C to 300 °C and had some antimony oxide (O_3Sb_2) impurity in samples MP350 and MP400 as confirmed by ICDD:98-000-1994. In the n-type samples, there were considerable phase changes at sintering temperatures 350 °C and 400 °C. In the tube furnace, the p-type materials have no peak shift for pristine, TP250, and TP300 samples. But for the TP350 and TP400 samples, there are several new oxidized impurity peaks, such as $Bi_2S_{0.15}Te_{2.85}$ and O_3Sb_2 confirmed by ICDD:98-061-7047, as shown in Fig. S1(d). For the n-type, the impure phases are similar to that observed in the box and microwave furnaces.

3.2. Compositional and morphological analysis

3.2.1. P-type

The Scanning Electron Microscopic (SEM) images of the p-type bismuth telluride samples both with and without sintering are shown in Fig. 2(a)–(d). The images depict how crystallization occurs with an increase in sintering temperatures. Fig. 2(a) represents the SEM image of the non-sintered p-type sample. It can be seen in Fig. 2(a) that the non-sintered samples had a layered structure with tellurium-rich phases. The thickness of each layer is in the range of ~10 nm. Fig. 2(b)–(d) indicates the crystallization process in the microwave furnace. The SEM images illustrating the crystallization process in conventional and tube furnaces are given in the Supplementary Data. It can be seen at 250 °C sintering temperature in the box and microwave furnace, the morphology and size were quite similar to the pristine p-type sample with an addition of few small ununiform micro-sized crystals. But in tube sintering, several micro-sized crystals were observed between the layers at 250 °C sintering temperature. Subsequently, the samples contained a mixture of nanocrystals and microcrystals (namely fine grains and coarse grains, respectively). The size of the sub-microns kept on
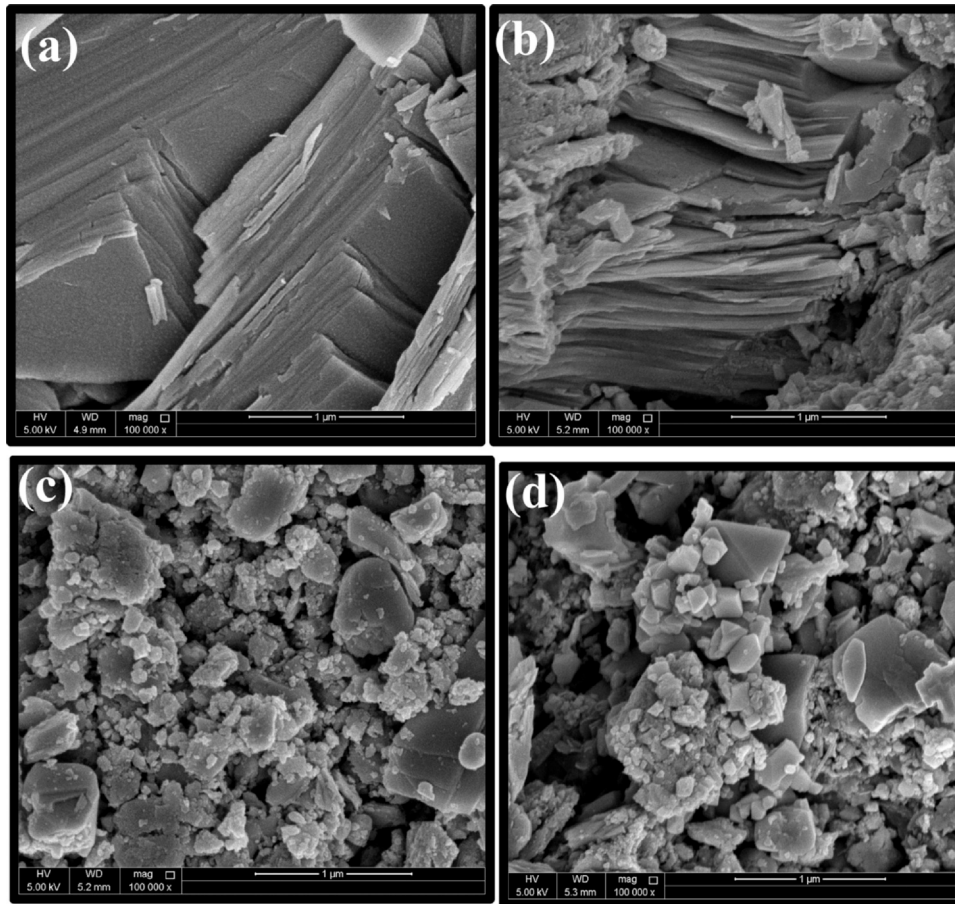
Fig. 2. Field emission scanning electron microscopy (FESEM) images at 1 µm of (a) pristine p-type Bi_2Te_3 sample, (b) MP250. (c) MP300, (d) MP350. Sub-microns of sizes less than 1 µm can be observed in the SEM images of samples sintered at 300 °C and 350 °C.

decreasing with an increase in sintering temperatures in all the sintering methods. That means with temperature increase, better and uniform finer grains were formed. This can be confirmed by the grain size calculated from XRD characterization data using the Debye-Scherrer formula given in the Supplementary Data. At sintering temperatures 300 °C and 350 °C in all the furnaces, the sub-microns were finer and uniformly distributed with sizes ranging between 500 and 900 nm, as shown in Fig. 2.

3.2.2. N-type

The Scanning Electron Microscopic (SEM) images of the n-type bismuth telluride samples both with and without sintering are shown in Fig. 3(a)–(d). The images indicate how crystallization occurs in different sintering at different temperatures. Fig. 3(a) represents the SEM image of the pristine n-type sample. It can be seen in Fig. 3(a), the pure sample had a layered structure with bismuth-rich phases. Fig. 3(b)–(d) indicates the crystallization process in the microwave furnace. The crystallization process in the conventional and tube furnace is given in the Supplementary Data. In p-type samples, the formation of micro-nano-sized crystals started roughly around 300 °C. But here, in the case of n-type samples, the crystallization started at a lower sintering temperature of 250 °C in all the sintering. At sintering temperatures 250 °C and 300 °C, the size and morphology of the samples consisted of unevenly and ununiform micro-sized crystals. In the box furnace at 250 °C, some layered structures can be observed. The SEM images also indicate that the samples consisted of both fine and coarse grains. Finer and finer particles were formed with an increase in sintering temperature. The

size of the sub-microns for the n-type samples ranges from 400 to 700 nm, as shown in Fig. 3.

3.3. Thermoelectric properties

3.3.1. DC electrical conductivity

The DC electrical conductivity of the pristine and the sintered samples was calibrated by Ossila four-point probe system. The software used was Ossila sheet resistance v1.0.01. The equipment applies direct current on the samples, and respective DC sheet resistances are measured. The DC conductivities of all the samples are given in Fig. 4. The p-type samples after sintering have become better conductors than the n-type samples with maximum conductivity values of 140 S/m and 47 S/m for p-type and n-type, respectively. For both p-type and n-type samples and all three types of sintering, the conductivities are higher at sintering temperatures 250 °C and 300 °C. The electrical conductivities have drastically reduced to the range 2–20 S/m for samples at temperatures 350 °C and 400 °C. The impurity in the samples sintered at 250 °C and 300 °C have no or negligible impurity concentration leading to high electrical conductivity values of 140 S/m. And for the samples sintered at 350 °C and 400 °C, the electrical conductivities were mostly from the bismuth oxide phases resulting in low values of 10 S/m. These oxide phases have restricted the free movement of electrons in the crystal of the samples [38,39]. Besides, the conductivities are higher for microwave and tube furnace-sintered samples due to lesser impurity concentration and oxidation in the chambers of the microwave and the presence of argon gas in the tube furnace.
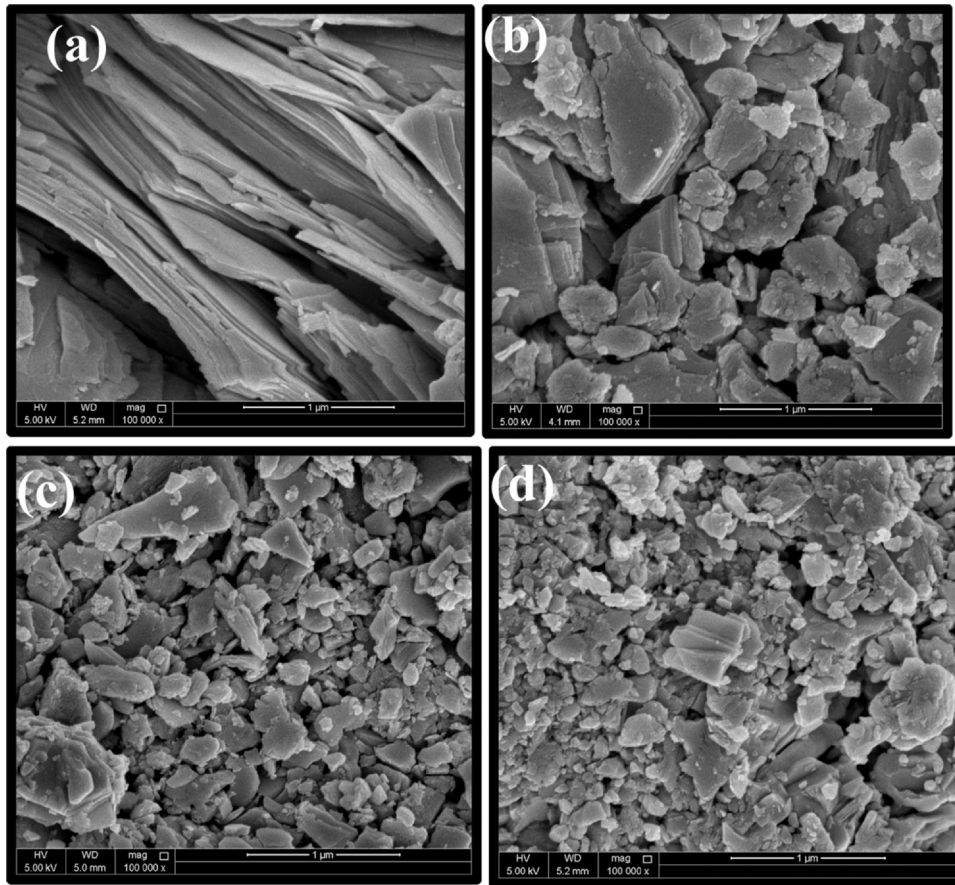
Fig. 3. Field emission scanning electron microscopy (FESEM) images at 1 µm of (a) Pristine n-type Bi_2Te_3 sample, (b) MN250. (c) MN300, (d) MN350. Sub-microns of sizes less than 1 µm can be observed in the SEM images of samples sintered at 300 °C and 350 °C.

3.3.2. Thermal conductivity

Two identical samples were prepared at each sintering temperature in the three furnaces, namely box, microwave, and tube. These samples were then tested for their thermal properties such as thermal conductivity, specific heat capacity, and thermal diffusivity by the Thermal constants analyzer (TCA) device. Fig. 5 depicts how the thermal conductivity of p-type and n-type varies with the

sintering temperatures. The thermal conductivities for the p-type samples are in the range 0.5–1.1 W/m/K, whereas, for the n-type, they are in the range 0.4–0.7 W/m/K. It is to be observed that the thermal conductivities are lower for n-type than p-type. The thermal conductivities are linearly proportional to the sintering temperatures. The samples sintered at 250 °C and 300 °C have very low conductivities compared to samples sintered at 350 °C and 400 °C.
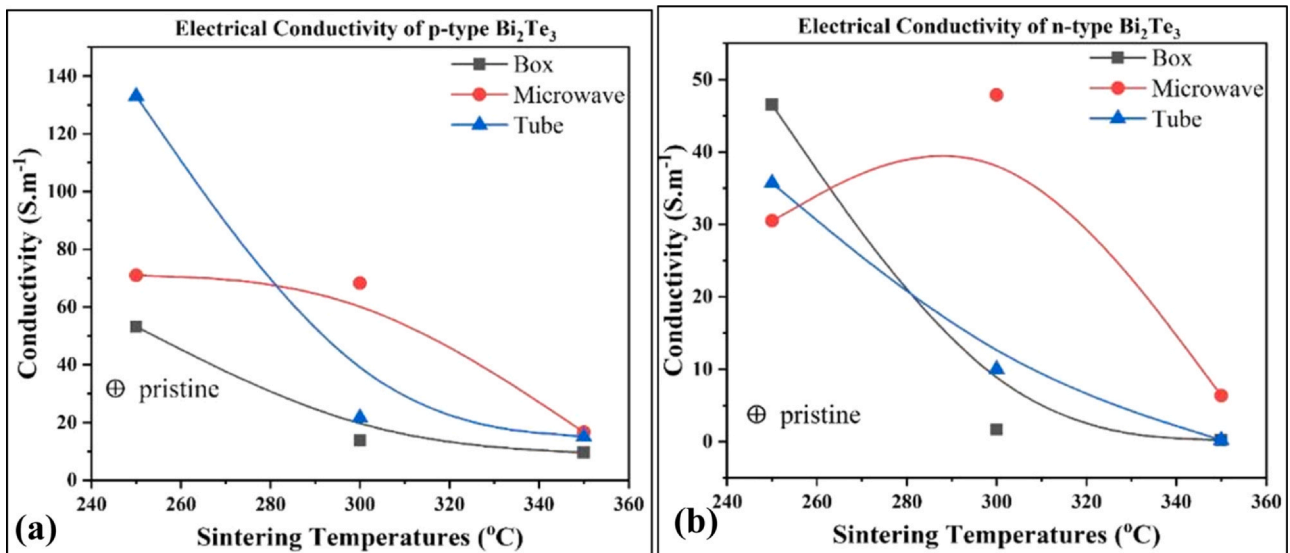

Fig. 4. The variation of DC electrical conductivities of (a) p-type and (b) n-type bismuth telluride samples in different furnaces at different sintering temperatures.
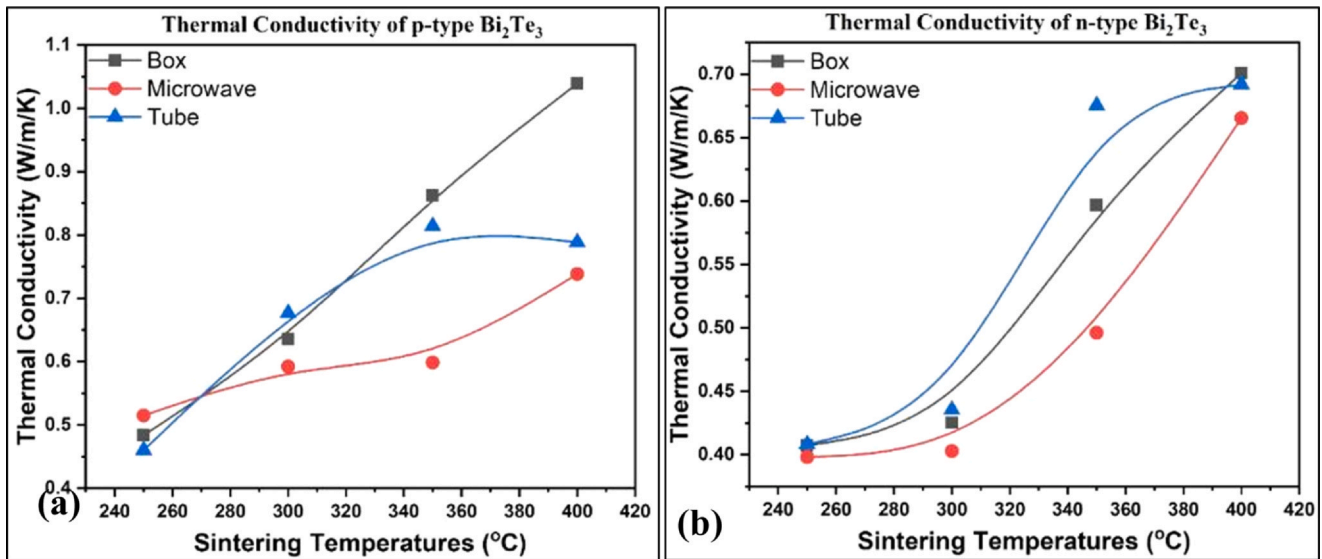
Fig. 5. The variation of thermal conductivities of (a) p-type and (b) n-type Bismuth telluride samples at different sintering temperatures.

The samples sintered in the box furnace have relatively high thermal conductivities of 1.1 W/m/K when compared to samples in other furnaces. The oxides of bismuth have very high thermal conductivities [40]. This is probably why the samples have high thermal conductivities at higher sintering temperatures (formation of oxide phases shown in the XRD data), especially in the box furnace.

3.4. Analysis of electrical properties through broadband dielectric spectroscopy

Broadband Dielectric spectroscopy is a powerful means to investigate dielectric material characterization since both the chain motion and conductivity can be monitored with respect to temperature and frequency in the same spectra [41]. It is also sometimes known as impedance spectroscopy and is used to study the physical and chemical properties of the materials and their interactions with electromagnetic radiation. Materials are made of atoms and molecules with electric charges that respond with the application of the electric field. The reactions may be in terms of state transition or

rotational motion, ultimately resulting in changes in macroscopic dielectric or electric behaviors in the materials. Gathering, sorting, and examining the dielectric behavior information of the materials is necessary for diverse fields such as material science, electronic chemistry, physical chemistry, and electrical engineering. Thus, using dielectric spectroscopy, we can effectively study the dielectric or electrical properties of thermoelectric materials related to the molecular structure, chemical composition, and phase morphology of the samples.

3.4.1. The variation of AC conductivity with temperature

Fig. 6 illustrates the AC electrical conductivities (σ_{ac}) at different frequencies 10 mHz, 1 Hz, 1 kHz, and 1 MHz for p-type and n-type Bi_2Te_3 samples sintered in the box furnace at 300 °C. The results show the variation of σ_{ac} with the temperature at different frequencies 10 mHz, 1 Hz, 1 kHz, and 1 MHz. The p-type samples demonstrated better σ_{ac} than n-type samples. The p-type samples sintered at 300 °C had the maximum electrical conductivity of 1.1 S/ cm. The conductivities had a very low or no change until the
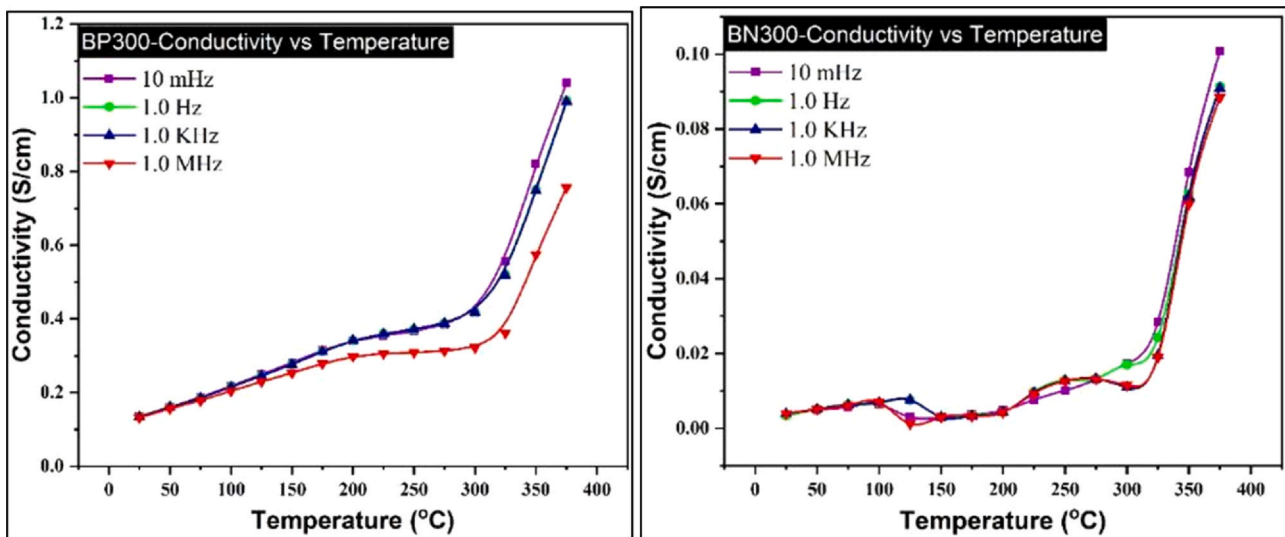

Fig. 6. Temperature dependence of electrical conductivity at frequencies 10 mHz, 1 Hz, 1 KHz, and 1 MHz for (a) p-type and (b) n-type Bi_2Te_3 samples sintered in box furnace at 300 °C. The conductivity increases with an increase in temperature and sudden spike can be observed in the range 350–400 °C. Also, the conductivity is high in case the frequency is 10 mHz.

measuring temperature 250 °C. Beyond 250 °C, there has been a sudden spike in the conductivities, probably due to the introduction of defects and improvement in the crystal size in the samples leading to increased carrier concentration and mobility [42]. The charge carriers at high temperatures are highly localized, leading to higher conduction through the hopping mechanism [43]. It also suggests that the pellets became highly conductive above 250 °C due to the availability of free majority charge carriers. There is a broad hump from 200 °C to 300 °C within the frequency range of 1 Hz to 1 MHz; however, the hump specified is rather very small or negligible for 10 mHz. Similar behavior has been previously reported in the case of CuO-doped SrTiO$_3$ [44].

Additionally, the coarse structures of samples sintered at 250 °C favor better electron transportation, as there is a decrease in the quantity of grain boundaries due to the formation of micro-sized structures. The movement of electrons is easier in coarse structures all the way through the electrically neutral grain boundaries that enhance the carrier transport in coarse and fine structures, unlike the phonon scattering [45]. However, even though the samples sintered at 350 °C and 400 °C had finer micro and nanostructures, the oxide impurity phases restricted the free movement of electrons, especially in the n-type samples, which had an abundance of bismuth resulting in a massive number of distinct bismuth oxide phases [38,39]. The samples in the microwave furnace and tube furnace had better σ_{ac} than the samples in the box furnace.

3.4.2. The variation of AC conductivity with frequency

The variation of AC conductivity with frequency is necessary to analyze the electrical conduction behavior in the bismuth telluride thermoelectrics. The capacitance and parallel conductance measurements were obtained in the spectrometer and Windeta software to calculate the appropriate frequency-dependent values of the AC conductivity σ_{ac}. The total conductivity is the sum of AC and DC conductivities, which is proposed by Jonscher's Universal power-law equation [46] given by

$$\sigma = \sigma_{dc} + A\omega^n \tag{3}$$

where σ_{dc} is the DC conductivity, which is frequency independent, A is the AC component or pre-exponential constant and ω is the angular frequency (2πf) and n is the power-law exponent of the mobile ions and ranges between 0 and 1. The σ_{ac} complies with the Almond-west universal power-law given by $\sigma_{ac} = A\omega^n$ [47]. The variation of AC conductivity through temperatures 25 °C to 375 °C with frequency f can be seen in Fig. 7. A typical conductivity vs. frequency spectrum exhibits three distinct regions, namely 1) low frequency dispersion, 2) an intermediate frequency plateau, and 3) an extended dispersion at

higher frequencies [41]. The low frequency (10 mHz–1 Hz) variation of the conductivities can be attributed to the dielectric polarization in the material [48]. This dielectric effect increases the capacitance in the material, thereby decreasing the AC conductivity that can be seen in the plots of Fig. 7. In the intermediate frequency range, the conductivity is almost independent of frequency and can be given by the DC conductivity. A sudden increase of the conductivity around 1 MHz indicates decreased polarization at higher oscillations in the high-frequency dispersive region. It is also noted that the conductivities increased with an increase in temperatures from 25 °C to 375 °C, implying the linear relationship of conductivity with temperature. This increase may be ascribed to the generation of multiple oxygen vacancies at higher temperatures and enhancement in the drift mobility of the charge carriers through thermal activation because of the increase in the hopping rate in the conduction mechanism [43]. The samples sintered at 300 °C showed a steady independent response to the frequency variations in conductivity. There is a rapid drop in conductivities in the samples at 350 °C from the low-frequency region to the intermediate frequency region.

3.4.3. The variation of dielectric permittivity storage with frequency

The variation of dielectric permittivity storage of as-prepared and sintered bismuth telluride samples with frequency through temperatures 25 °C to 375 °C are depicted in Fig. 8. The sintering conditions and temperatures influence the physical properties of the sample pellets, which in turn affects their dielectric properties. The electron transport properties are affected, making it an absolute necessity to investigate the influence of temperature and sintering method on the dielectric constant, dielectric loss, and electric modulus of the referenced samples. The frequency-dependent dielectric parameter is termed by the complex form of permittivity given by

$$\varepsilon^* = \varepsilon' - j\varepsilon'' \tag{4}$$

where real part ε' is the relative dielectric permittivity or dielectric permittivity constant or storage and imaginary part ε'' is the dielectric loss. The dielectric constant can be calculated from the capacitance C and is given by

$$\varepsilon' = C \times \left(\frac{d}{A}\right) \tag{5}$$

where A is the surface area of the sample (πr^2;r is the radius) and d is the thickness of the sample.

The dielectric loss ε'' can be calculated from the measured conductance (G) with the following expression:
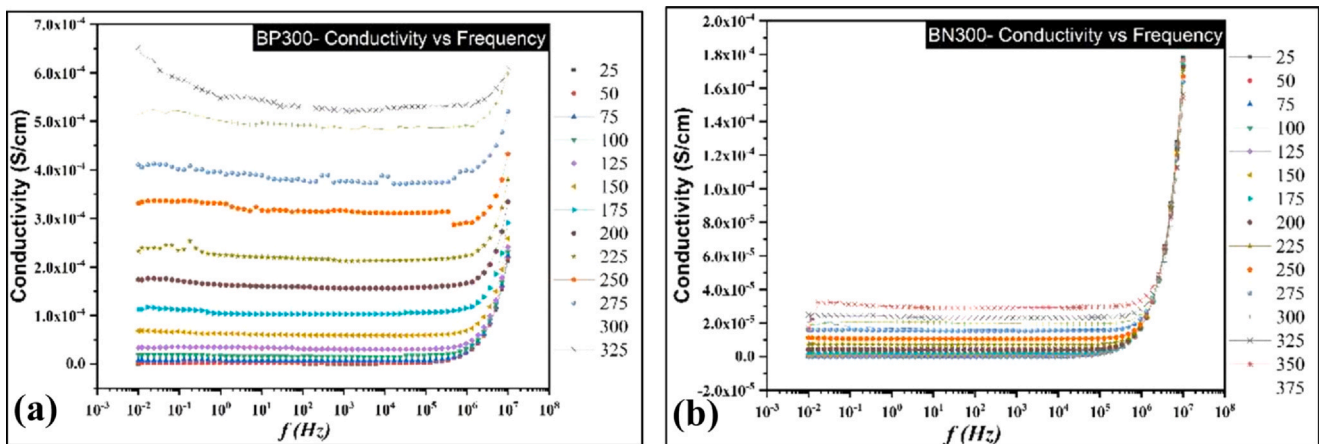

Fig. 7. Frequency dependence of electrical conductivity in the temperature range 25 °C to 375 °C for (a) p-type and (b) n-type Bi$_2$Te$_3$ samples sintered in box furnace at 300 °C. The conductivity is high at temperature 375 °C. A spike in AC conductivity can be observed at higher frequencies.
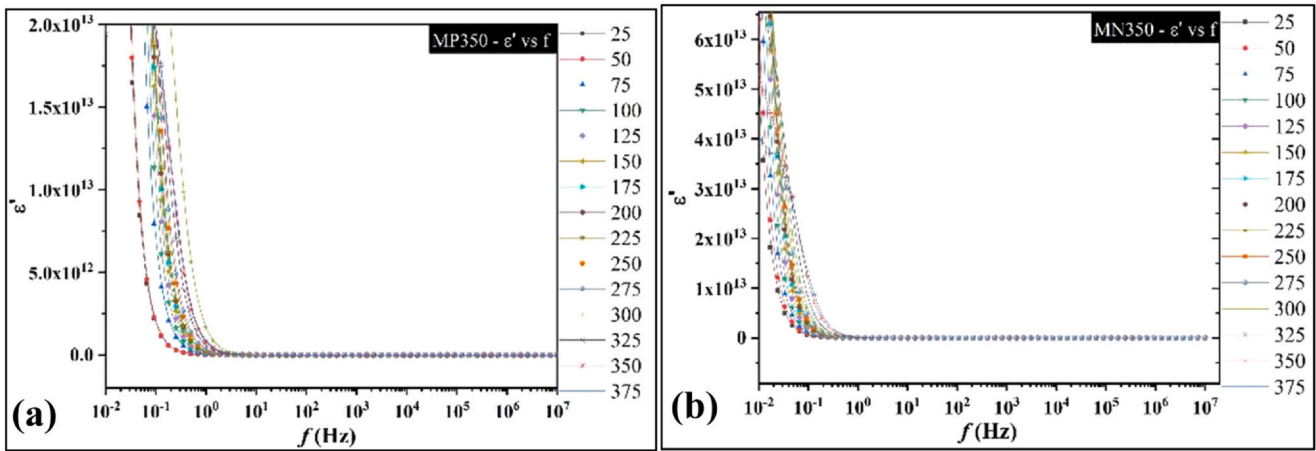
Fig. 8. Frequency dependence of dielectric storage in the temperature range 25 °C to 375 °C for (a) p-type and (b) n-type Bi$_2$Te$_3$ samples sintered in microwave furnace sintered at 350 °C.

$$\varepsilon'' = G \times \left(\frac{d}{\varepsilon_o \omega A} \right) \tag{6}$$

where ε_o is the permittivity in free space.

The plots in Fig. 8 show that the dielectric storage decreases with increasing frequency. This may be related to the tendency of dipoles in the sample pellets to orient themselves in line with the applied electric field direction [49]. On the other hand, the values of the dielectric storage remained constant with a change in frequency in the higher frequency range. The temperature change did not have much effect on the characteristics except with a slight shift in the transient frequencies. This trend remained the same for all the samples, with some variation in the magnitude of the dielectric constant values. It could be attributed to the fact that the rotation of dipoles is hindered by higher frequencies making it hard for the dipoles to reorient [49]. The dielectric constant rapidly decreased with an increase in frequency and remained very low and almost constant after the 1 Hz frequency. This dielectric dispersion was larger for higher temperatures and decreased with temperature decrease. This dielectric behavior can be attributed to the mechanism of the polarization process in bismuth tellurides quite similar to that of the conduction process.

3.4.4. The variation of dielectric loss with frequency

Dielectric permittivity loss can be loosely stated as the loss of energy when heating a material when the varying or AC electric field is applied. The dielectric losses rely on the frequency of the electric field applied and the permittivity or dielectric feature of the material.

Fig. 9 shows the changes in the dielectric loss of the as-prepared and sintered bismuth telluride samples in the electromagnetic spectrum at various temperatures from 25 °C to 375 °C. ε'' is very high at low frequencies correspondent to the DC electrical conductivities, probably from the free charge polarization within the sample material [48]. This dielectric loss decreased linearly with an increase in frequency. So, it can be said that the dielectric loss increases with a temperature rise and decreases with an increase in frequency. The relation of this dielectric loss ε'' with frequency can be given from the power law [50],

$$\varepsilon'' = B. \, \omega^m \tag{7}$$

where B and m are constant and frequency power factor, respectively. The plots of log ε'' versus log(freq) or log(ω) depict straight lines at different temperatures. The m values can be obtained from the slopes of the lines at various temperatures using Eq. (7). It can be
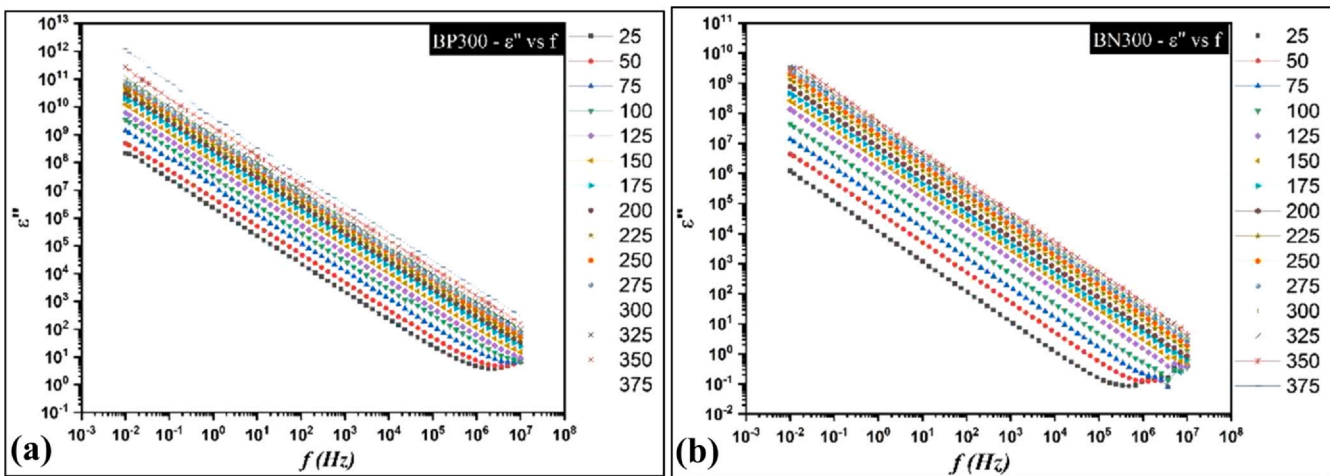

Fig. 9. Frequency dependence of log of imaginary part of permittivity or dielectric loss in the temperature range 25 °C to 375 °C for (a) p-type and (b) n-type Bi$_2$Te$_3$ samples sintered in box furnace at 300 °C.

observed that this m value tends to decrease with a temperature rise. The response of dielectric loss on low frequency side corresponds to the low AC conductivity and electric modulus values in this frequency range. The response of AC conductivity at low frequency is DC conductivity. This response corresponds to typical Debye relation given by $\sigma dc = 2\pi f \varepsilon_o \varepsilon''$ [51].

4. Conclusion

In this work, we have treated p-type and n-type bismuth telluride nanocrystals using conventional, microwave, and tube sintering. The XRD and SEM characterization were done to study the structural and microscopic properties of the treated materials. The DC electrical conductivity and thermal conductivity were determined by the 4-point probe method and TCA test, respectively. The dielectric characterization was done using dielectric spectroscopy. The XRD analysis showed that the prepared materials remained stable with a single-phase at sintering temperatures 250 °C and 300 °C. However, beyond 300 °C, phase change occurred with the appearance of oxide impurities at 350–400 °C sintering temperatures. Also, the DC electrical conductivity decreased as the sintering temperature went from 250 °C to 400 °C with an increase in coarse and crystalline structures. On the contrary, the thermal conductivity increased with an increase in sintering temperatures. The broadband dielectric spectroscopy confirmed that the conduction behavior in the samples was from the hopping mechanism, and the samples exhibited characteristics more similar to glass. Therefore, the samples had an exceptionally ultra-low thermal conductivity of approximately 0.4 W/m/K. The microwave furnace samples demonstrated better thermoelectric properties among all the sintering with an optimum annealing temperature of 250 °C. However, the higher oxidation levels have restricted the characteristics of the materials that can be avoided by acute control of the sintering atmospheres.

CRediT authorship contribution statement

Farheen F. Jaldurgam: Methodology, Data curation, Writing - original draft. **Zubair Ahmad:** Conceptualization, Methodology, Supervision, Validation, Writing - review & editing. **Farid Touati:** Writing - review & editing. **Abdulla Al Ashraf**: Data curation. **Abdul Shakoor**: Validation, Writing - review & editing. **Jolly Bhadra**: Writing - review & editing. **Noora J. Al-Thani**: Writing - review & editing. **Dong Suk Han**: Writing - review & editing. **Talal Altahtamouni:** Conceptualization, Writing - review & editing.

Declaration of Competing Interest

There is no conflict of interest.

Acknowledgments

Appendix A. Supporting information

Supplementary data associated with this article can be found in the online version at doi:10.1016/j.jallcom.2021.160256.

References

[1] Z.-G. Chen, G. Han, L. Yang, L. Cheng, J. Zou, Nanostructured thermoelectric materials: current research and future challenge, Prog. Nat. Sci. Mater. Int. 22 (2012) 535–549.

[2] D.M. Rowe, CRC Handbook of Thermoelectrics, CRC Press, 2018.

[3] G. Tan, S. Hao, J. Zhao, C. Wolverton, M.G. Kanatzidis, High thermoelectric performance in electron-doped AgBi3S5 with ultralow thermal conductivity, J. Am. Chem. Soc. 139 (2017) 6467–6473.

[4] S. Roychowdhury, M.K. Jana, J. Pan, S.N. Guin, D. Sanyal, U.V. Waghmare, K. Biswas, Soft phonon modes leading to ultralow thermal conductivity and high thermoelectric performance in AgCuTe, Angew. Chem. 130 (2018) 4107–4111.

[5] P.C. Wei, C.N. Liao, H.J. Wu, D. Yang, J. He, G.V. Biesold-McGee, S. Liang, W.T. Yen, X. Tang, J.W. Yeh, Thermodynamic routes to ultralow thermal conductivity and high thermoelectric performance, Adv. Mater. 32 (2020) 1906457.

[6] P. Liu, G. Chen, Y. Cui, H. Zhang, F. Xiao, L. Wang, H. Nakano, High temperature electrical conductivity and thermoelectric power of NaxCoO2, Solid State Ion. 179 (2008) 2308–2312.

[7] G.J. Snyder, E.S. Toberer, Complex thermoelectric materials, Mater. Sustain. Energy. (2011) 101–110 (a collection of peer-reviewed research and review articles from Nature Publishing Group).

[8] S. Mishra, S. Satpathy, O. Jepsen, Electronic structure and thermoelectric properties of bismuth telluride and bismuth selenide, J. Phys. Condens. Matter 9 (1997) 461–470.

[9] X. Zhao, X. Ji, Y. Zhang, T. Zhu, J. Tu, X. Zhang, Bismuth telluride nanotubes and the effects on the thermoelectric properties of nanotube-containing nanocomposites, Appl. Phys. Lett. 86 (2005) 062111.

[10] I.T. Witting, T.C. Chasapis, F. Ricci, M. Peters, N.A. Heinz, G. Hautier, G.J. Snyder, The thermoelectric properties of bismuth telluride, Adv. Electron. Mater. 5 (2019) 1800904.

[11] L. Hu, H. Wu, T. Zhu, C. Fu, J. He, P. Ying, X. Zhao, Tuning multiscale microstructures to enhance thermoelectric performance of n-type Bismuth-Telluride-based solid solutions, Adv. Energy Mater. 5 (2015) 1500411.

[12] R. Zhai, L. Hu, H. Wu, Z. Xu, T.-J. Zhu, X.-B. Zhao, Enhancing thermoelectric performance of n-type hot deformed bismuth-telluride-based solid solutions by nonstoichiometry-mediated intrinsic point defects, ACS Appl. Mater. Interfaces 9 (2017) 28577–28585.

[13] L. Hu, T. Zhu, X. Liu, X. Zhao, Point defect engineering of high-performance bismuth-telluride-based thermoelectric materials, Adv. Funct. Mater. 24 (2014) 5211–5218.

[14] J. Drabble, C. Goodman, Chemical bonding in bismuth telluride, J. Phys. Chem. Solids 5 (1958) 142–144.

[15] H. Goldsmid, Recent studies of bismuth telluride and its alloys, J. Appl. Phys. 32 (1961) 2198–2202.

[16] H. Mamur, M. Bhuiyan, F. Korkmaz, M. Nil, A review on bismuth telluride (Bi2Te3) nanostructure for thermoelectric applications, Renew. Sustain. Energy Rev. 82 (2018) 4159–4169.

[17] G. Mahan, Figure of merit for thermoelectrics, J. Appl. Phys. 65 (1989) 1578–1583.

[18] C. Hollar, Z. Lin, M. Kongara, T. Varghese, C. Karthik, J. Schimpf, J. Eixenberger, P.H. Davis, Y. Wu, X. Duan, High-performance flexible bismuth telluride thin film from solution processed colloidal nanoplates, Adv. Mater. Technol. 5 (2020) 2000600.

[19] Y. Wu, R. Zhai, T. Zhu, X. Zhao, Enhancing room temperature thermoelectric performance of n-type polycrystalline bismuth-telluride-based alloys via Ag doping and hot deformation, Mater. Today Phys. 2 (2017) 62–68.

[20] F. Li, R. Zhai, Y. Wu, Z. Xu, X. Zhao, T. Zhu, Enhanced thermoelectric performance of n-type bismuth-telluride-based alloys via In alloying and hot deformation for mid-temperature power generation, J. Mater. 4 (2018) 208–214.

[21] M. Takashiri, K. Miyazaki, S. Tanaka, J. Kurosaki, D. Nagai, H. Tsukamoto, Effect of grain size on thermoelectric properties of n-type nanocrystalline bismuth-telluride based thin films, J. Appl. Phys. 104 (2008) 084302.

[22] K. Singkaselit, A. Sakulkalavek, R. Sakdanuphab, Effects of annealing temperature on the structural, mechanical and electrical properties of flexible bismuth telluride thin films prepared by high-pressure RF magnetron sputtering, Adv. Nat. Sci. Nanosci. Nanotechnol. 8 (2017) 035002.

[23] L. Ren, X. Qi, Y. Liu, G. Hao, Z. Huang, X. Zou, L. Yang, J. Li, J. Zhong, Large-scale production of ultrathin topological insulator bismuth telluride nanosheets by a hydrothermal intercalation and exfoliation route, J. Mater. Chem. 22 (2012) 4921–4926.

[24] D. Teweldebrhan, V. Goyal, M. Rahman, A.A. Balandin, Atomically-thin crystalline films and ribbons of bismuth telluride, Appl. Phys. Lett. 96 (2010) 053107.

[25] A. Ubelis, Temperature dependence of the saturated vapor pressure of tellurium, J. Eng. Phys. 42 (1982) 309–315.

[26] Z. Shi, Q. Zhao, B. Guo, T. Ji, H. Wang, A review on processing polycrystalline magnesium aluminate spinel (MgAl2O4): sintering techniques, material properties and machinability, Mater. Des. 193 (2020) 108858.

[27] X.-y Wang, H.-j Wang, B. Xiang, H.-j Shang, B. Zhu, Y. Yu, H. Jin, R.-f Zhao, Z.-y Huang, L.-j Liu, Attaining reduced lattice thermal conductivity and enhanced electrical conductivity in as-sintered pure n-type Bi 2 Te 3 alloy, J. Mater. Sci. 54 (2019) 4788–4797.

[28] C.-C. Lin, R. Lydia, J.H. Yun, H.S. Lee, J.S. Rhyee, Extremely low lattice thermal conductivity and point defect scattering of phonons in Ag-doped (SnSe) 1−x (SnS) x compounds, Chem. Mater. 29 (2017) 5344–5352.

[29] R.H. Castro, Overview of conventional sintering, Sintering, Springer, 2012, pp. 1–16.

[30] M. Oghbaei, O. Mirzaee, Microwave versus conventional sintering: a review of fundamentals, advantages and applications, J. Alloy. Compd. 494 (2010) 175–189.

[31] B. Zhou, Y. Zhao, L. Pu, J.-J. Zhu, Microwave-assisted synthesis of nanocrystalline Bi2Te3, Mater. Chem. Phys. 96 (2006) 192–196.

[32] D.H. Kim, C. Kim, S.H. Heo, H. Kim, Influence of powder morphology on thermoelectric anisotropy of spark-plasma-sintered Bi–Te-based thermoelectric materials, Acta Mater. 59 (2011) 405–411.

[33] D. Kong, J.C. Randel, H. Peng, J.J. Cha, S. Meister, K. Lai, Y. Chen, Z.-X. Shen, H.C. Manoharan, Y. Cui, Topological insulator nanowires and nanoribbons, Nano Lett. 10 (2010) 329–333.

[34] E. Ashalley, H. Chen, X. Tong, H. Li, Z.M. Wang, Bismuth telluride nanostructures: preparation, thermoelectric properties and topological insulating effect, Front. Mater. Sci. 9 (2015) 103–125.

[35] P. Anandan, M. Omprakash, M. Azhagurajan, M. Arivanandhan, D.R. Babu, T. Koyama, Y. Hayakawa, Tailoring bismuth telluride nanostructures using a scalable sintering process and their thermoelectric properties, CrystEngComm 16 (2014) 7956–7962.

[36] E.M. Modan, A.G. Plăiașu, Advantages and disadvantages of chemical methods in the elaboration of nanomaterials, Ann. "Dunarea de Jos" Univ. Galati. Fascicle IX Metall. Mater. Sci. 43 (2020) 53–60.

[37] U. Holzwarth, N. Gibson, The Scherrer equation versus the'Debye-Scherrer equation', Nat. Nanotechnol. 6 (2011) 534 534-534.

[38] D. Smyth, Electrical conductivity in ceramics: a review, Ceram. Microstruct. 86 (1987) 643–655.

[39] Y.-P. Wang, S.-S. Li, W.-X. Ji, C.-W. Zhang, P. Li, P.-J. Wang, Bismuth oxide film: a promising room-temperature quantum spin Hall insulator, J. Phys. Condens. Matter 30 (2018) 105303.

[40] N. Anisimova, G. Bordovsky, V. Bordovsky, V. Seldayev, Electrical and thermal properties of Bi2O3, PbO and mixed oxides of Bi2O3-PbO system, in: Proceedings of the 2004 IEEE International Conference on Solid Dielectrics (Toulouse, July 5–9, 2004), 2004.

[41] F. Kremer, A. Schönhals, Broadband Dielectric Spectroscopy, Springer Science & Business Media, 2002.

[42] Q. Zhang, Q. Song, X. Wang, J. Sun, Q. Zhu, K. Dahal, X. Lin, F. Cao, J. Zhou, S. Chen, Deep defect level engineering: a strategy of optimizing the carrier concentration for high thermoelectric performance, Energy Environ. Sci. 11 (2018) 933–940.

[43] S. Pal, A. Banerjee, E. Rozenberg, B. Chaudhuri, Polaron hopping conduction and thermoelectric power in LaMnO 3+ δ, J. Appl. Phys. 89 (2001) 4955–4961.

[44] K.C.B. Naidu, T.S. Sarmash, M. Maddaiah, V.N. Reddy, T. Subbarao, Structural and dielectric properties of CuO-doped SrTiO3 ceramics, in: Proceedings of the AIP Conference Proceedings, AIP Publishing LLC, 2015, pp. 040001.

[45] J. Cao, D. Ekren, Y. Peng, F. Azough, I.A. Kinloch, R. Freer, Modulation of charge transport at grain boundaries in SrTiO3: toward a high thermoelectric power factor at room temperature, ACS Appl. Mater. Interfaces (2021).

[46] A. Jonscher, A new understanding of the dielectric relaxation of solids, J. Mater. Sci. 16 (1981) 2037–2060.

[47] A.K. Jonscher, The 'universal'dielectric response, Nature 267 (1977) 673–679.

[48] T. Dakin, Conduction and polarization mechanisms and trends in dielectric, IEEE Electr. Insul. Mag. 22 (2006) 11–28.

[49] H. Bouaamlat, N. Hadi, N. Belghiti, H. Sadki, M. Naciri Bennani, F. Abdi, T.-d Lamcharfi, M. Bouachrine, M. Abarkan, Dielectric properties, AC conductivity, and electric modulus analysis of bulk ethylcarbazole-terphenyl, Adv. Mater. Sci. Eng. 2020 (2020) 1–8.

[50] M. Seyam, A. Bekheet, A. Elfalaky, AC conductivity and dielectric properties of In2S3 films, Eur. Phys. J. Appl. Phys. 16 (2001) 99–104.

[51] M.A. Mahdy, I. El Zawawi, G.M. Turky, Lead telluride nanocrystalline thin films: structure, optical characterization and a broadband dielectric spectroscopy study, Curr. Appl. Phys. 19 (2019) 787–793.